⌘ *Author's Choice*

Electron microscopy snapshots of single particles from single cells

Xiunan Yi[‡§¶1], Eric J. Verbeke[‡§¶1], Yiran Chang[‡§¶1], Daniel J. Dickinson[‡§¶2,3], and ⬤ David W. Taylor[‡§¶‖3,4]

From the ‡Department of Molecular Biosciences, §Center for Systems and Synthetic Biology, and the ¶Institute for Cellular and Molecular Biology, University of Texas at Austin, Austin, Texas 78712 and ‖LIVESTRONG Cancer Institute, Dell Medical School, Austin, Texas 78712

Edited by Karin Musier-Forsyth

Cryo-electron microscopy (cryo-EM) has become an indispensable tool for structural studies of biological macromolecules. Two additional predominant methods are available for studying the architectures of multiprotein complexes: 1) single-particle analysis of purified samples and 2) tomography of whole cells or cell sections. The former can produce high-resolution structures but is limited to highly purified samples, whereas the latter can capture proteins in their native state but has a low signal-to-noise ratio and yields lower-resolution structures. Here, we present a simple, adaptable method combining microfluidic single-cell extraction with single-particle analysis by EM to characterize protein complexes from individual *Caenorhabditis elegans* embryos. Using this approach, we uncover 3D structures of ribosomes directly from single embryo extracts. Moreover, we investigated structural dynamics during development by counting the number of ribosomes per polysome in early and late embryos. This approach has significant potential applications for counting protein complexes and studying protein architectures from single cells in developmental, evolutionary, and disease contexts.

Cell behavior is fundamentally dependent on the activities of macromolecular machines. These machines, comprised of protein (and sometimes RNA) subunits, are responsible for catalytic, structural, and regulatory activities that allow cells to function. Structural biology, by revealing the physical architecture of macromolecules and their assemblies, plays a critical role in efforts to understand how molecular mechanisms contribute to cell behavior *in vivo*.

A crucial feature of most living cells is their ability to adjust their behavior in response to their environment. In a developmental context, cells respond to chemical and mechanical cues from neighboring cells and tissues to coordinate their behavior with their neighbors and to assemble functional tissues. A major goal of developmental biology studies is to understand the molecular mechanisms of these interactions—that is, how dynamic behaviors of macromolecular machines give rise to cell behaviors that support proper organismal development.

Recently, single-cell nucleic acid sequencing approaches have revolutionized developmental studies by allowing gene expression to be interrogated with unprecedented spatiotemporal resolution (1). Such experiments are powerful because they reveal which genes are expressed in which cells at a particular point in development and can thus provide insights into signaling dynamics, mechanisms of cell state changes (*e.g.* cellular differentiation), and levels of heterogeneity between individual cells. However, sequencing approaches do not shed light on the molecular states or interactions of cellular proteins. A few studies have begun to extend a single-cell approach to biochemical studies of proteins and protein complexes. For example, Huang and Zare (2) described a sophisticated microfluidic device for counting protein molecules in single-cell lysates. Allbritton and co-workers (3, 4) have developed capillary electrophoreses methods for measuring enzyme activities in whole-cell lysates. Most recently, Dickinson *et al.* (5) used microfluidic lysis followed by single-molecule pulldown and TIRF[5] microscopy to measure the abundance of protein complexes in single cells. This s̲ingle-c̲ell, s̲ingle-m̲olecule p̲ulldown (sc-SiMPull) approach was sufficiently sensitive to reveal regulated changes in protein– interactions that occurred over ~5 min during development of the *Caenorhabditis elegans* zygote. Thus, single-cell biochemical approaches have the potential to uncover dynamics of macromolecular machines in cell or tissue samples obtained directly from developing embryos.

Although still in their infancy, the initial success of these single-cell biochemical methods raises the question of whether a single-cell approach could be extended to macro-

This article contains Video S1 and Figs. S1–S4.

The EM reconstructions of the 40S, 60S, and 80S have been deposited into the Electron Microscopy Data Bank with accession codes EMD-0398, EMD-0399, and EMD-0400, respectively.

[1] These authors contributed equally to this work.
[2] To whom correspondence may be addressed: Dept. of Molecular Biosciences, University of Texas at Austin, Austin, TX 78712. Tel.: 512-232-2916; E-mail: daniel.dickinson@austin.utexas.edu.
[3] These authors are CPRIT Scholars supported by Cancer Prevention and Research Institute of Texas Grants RR160088 and RR170054.
[4] To whom correspondence may be addressed: Dept. of Molecular Biosciences, University of Texas at Austin, Austin, TX 78712. Tel.: 512-471-9156; E-mail: dtaylor@utexas.edu.

[5] The abbreviations used are: TIRF, total internal reflection fluorescence; cryo-EM, cryo-electron microscopy; PDMS, polydimethylsiloxane; MS, mass spectrometry.

ASBMB

molecular structure determination. Such an approach could overcome a classical limitation of structural biology: its need for highly purified, homogenous proteins (or protein complexes) that represent only a single snapshot from the ensemble of structures that are likely present in cells. Moreover, the ability to determine structures of proteins obtained directly from cells engaged in development would represent a significant step toward the goal of linking the structural dynamics of molecular machines to their cellular and developmental consequences.

One approach to single-cell structural studies is electron tomography. This allows for the study of cell morphologies (6), and in some cases, can be used to reconstruct 3D models directly from native cells (7). However, because of the sensitivity of biological specimens to electron dose, tomographic approaches routinely lead to low- or intermediate-resolution structures of complexes in single cells using subtomogram averaging techniques. The advent of phase plates for EM has revolutionized the information contact extractable from tomograms, but high-resolution structures of less-abundant complexes remain elusive.

Alternatively, single-particle cryo-electron microscopy (cryo-EM) is now capable of routinely achieving high-resolution structures of highly purified samples because of advances in hardware (8) and software (9, 10). We and others have recently extended single-particle EM techniques to study heterogenous mixtures from biochemically fractionated cell lysate (11, 12). Although these shotgun-EM approaches are able to sort through the heterogeneity of macromolecules, they still rely on a large quantity of cells and mass spectrometry (MS) to characterize the contents of the sample. Furthermore, direct investigation of proteins at the single-cell level has remained a challenging problem for proteomic studies. This poses a unique challenge to structural studies of single cells.

Some efforts toward applying single-particle EM methods to single cells have been made (13, 14) that importantly demonstrated the feasibility of extracting material from single cells for EM analysis. However, this earlier work required a complicated apparatus and has not yet yielded any 3D structures of macromolecular complexes. Here, we propose an alternative approach for combining single-cell lysis with EM to investigate macromolecular structures. Our method is technically simpler than previous approaches but is able to directly visualize the contents of a single cell. After computationally classifying the particles from cell lysate, we uncover the 3D structures of 40S and 60S ribosomes from disperse particles and the structure of an 80S ribosome from polysomes. Because we chose to apply our approach to a developmental model system (*C. elegans* zygotes and embryos), we are able to obtain structural information from embryos at specific developmental stages. In one application, we find that the number of ribosomes per polysome remains consistent between early- and late-stage embryos. These results demonstrate the potential of EM for structural characterization of unpurified macromolecular machines obtained from samples as small as a single cell.
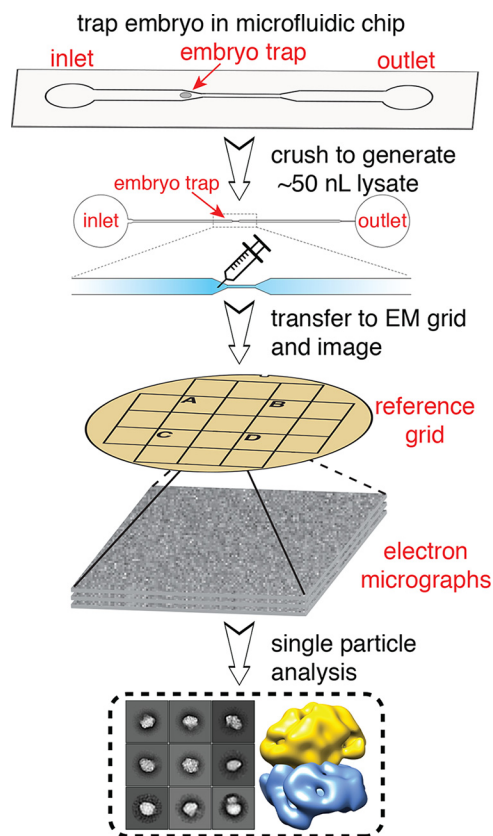

Figure 1. Schematic of single-cell structural biology approach. Single *C. elegans* embryos are trapped in a microfluidic device. After the embryo is crushed, the lysate is extracted using a fine needle and applied to a specific area of an EM grid using a stereoscope. The same area is then visualized using EM, and single-particle analysis is applied for structure determination.

Results

Extracting macromolecules from single embryos

Our primary goal in this study was to determine whether imaging of single-cell lysates with EM could yield sufficient, high-quality particles for 3D structure determination. To obtain intact, native particles from single cells, *C. elegans* zygotes (*i.e.* 1-cell embryos) were trapped and lysed using microfluidic chambers (Fig. 1) (see "Experimental Procedures"). We then transferred the cell lysates (a volume of ~50 nl) from the microfluidic channels to EM grids using a glass needle (Video S1) (see "Experimental Procedures"). Because of the small volume, which was insufficient to coat an entire grid, we used reference grids containing alphanumeric markers to locate the placement of our samples under both the dissecting scope and the electron microscope. Each reference grid was then conventionally stained using 2% (w/v) uranyl acetate. We chose to use negative stain EM for its high signal-to-noise ratio to more accurately assess our ability to identify single particles from individual cell lysates. Each grid was then examined by transmission EM to identify grid squares that contained cellular protein particles embedded in stain.

To demonstrate our ability to capture small volumes of samples on EM grids, we first transferred samples of a purified protein kinase (15) from our microfluidic device to an EM grid for visualization, resulting in successful detection of the kinase (Fig. S1). We then performed our transfer technique on lysates
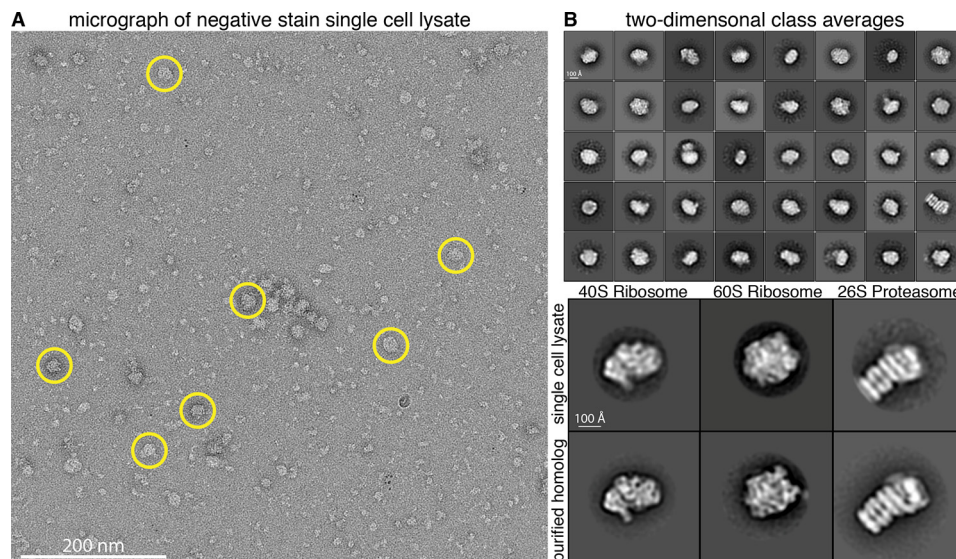
A micrograph of negative stain single cell lysate

B two-dimensonal class averages

40S Ribosome   60S Ribosome   26S Proteasome

single cell lysate

purified homolog

Figure 2. Single-particle analysis of extracts from single cells. *A*, representative raw electron micrograph of negatively stained single-cell lysates. Micrographs show monodisperse particles of varying size. *Circled* particles are representative of the larger particles (~150–300 Å in diameter) used for subsequent 2D and 3D classification. *B*, *top panel*, reference-free 2D alignment and classification of a subset of the ~50,000 particles picked from single-cell extract. Classes are sorted in order of decreasing abundance. Box size is 576 × 576 Å. *Bottom panel*, alignment of 2D class averages from single-cell extract to purified homologs.

from seven independent single embryos sampled at different developmental stages, three from zygotes and four from later-stage, multicell embryos. Micrographs of single-cell extract across different embryos show a reproducible mixture of heterogeneous particles that span an order of magnitude in size (Fig. S1). These data allowed us to investigate the dynamics of protein complexes at the single-cell/embryo level between different developmental stages of *C. elegans* zygotes.

EM of extract from a single C. elegans embryo

Raw micrographs collected at the locations where embryo lysate had been applied to the EM grid showed distinct, monodisperse particles with varying sizes and distinct shapes. The results unambiguously show that we were able to retrieve cellular contents from our microfluidic lysis chips for subsequent imaging by EM, although we cannot exclude the possibility that some particles may fail to adhere to the grid and be lost during sample preparation (Fig. 2A). We collected ~1,400 micrographs between the seven samples. Although small particles were abundant in our micrographs (Fig. S1), we first chose to analyze large particles (~150–300 Å in diameter), which were easily recognizable and appeared relatively homogeneous. After manually selecting ~10,000 large particles from a subset of micrographs, we generated reference-free 2D class averages that were subsequently used as templates for automated picking of particles from all micrographs. Using this template picking scheme, ~80,000 large particles were selected from ~1,400 micrographs and used for reference-free 2D alignment and classification. 2D class averages with distinct structural features were generated from ~50,000 particles after removing junk particles (*e.g.* detergent micelles, irregular small particles, two nearby particles, or particles in aggregates) from the data (Fig. 2B, *top panel*).

To obtain insight into the possible identities of these particles, we used publicly available RNA-seq data from *C. elegans* 1-cell embryos (16, 17) to inform us about which proteins are likely to be highly expressed. 34 ribosomal protein transcripts and 4 proteasomal protein transcripts were among the 200 most abundant transcripts, suggesting these protein complexes were likely to appear in our micrographs (Fig. S2) (16, 17). None of the other 200 most highly expressed proteins are known subunits of large (megadalton) macromolecular complexes, suggesting that ribosomes and proteasomes should be the most abundant large particles in our data set. We therefore performed pairwise cross-correlations of our 2D class averages with 2D class averages of purified 40S ribosome, 60S ribosome (18), and 26S proteasome (19) from *Saccharomyces cerevisiae* to look for structural similarities. The alignment revealed several classes with similar features between our single-cell lysate and the known, purified structures, suggesting the identity of several projections in our sample were in fact the 40S ribosome, 60S ribosome, and 26S proteasome (Fig. 2B, *bottom panel*). This initial 2D classification proved it is possible to obtain structural information from intact protein complexes extracted from lysates of single cells.

Capturing ribosome dynamics in polysomes

Intriguingly, our raw micrographs revealed densely packed clusters of ribosome-like particles (Fig. 3A). These ribosome-like particles appeared in organized arrays with a similar appearance to polysomes from *Escherichia coli* (20) and wheat germ (21). Polysomes consist of a pool of actively translating ribosomes on an mRNA transcript. This suggested that our single-cell EM method is capable of capturing protein–mRNA interactions in the cell.

In *C. elegans*, zygotic transcription begins at the four-cell stage (22, 23); prior to this, development is driven by maternal RNA and proteins. We were curious whether polysome architecture would change as a consequence of new zygotic transcription. Because we observed polysomes in both early- and late-stage embryos (before and after the onset of zygotic transcription), we addressed this question by counting the number
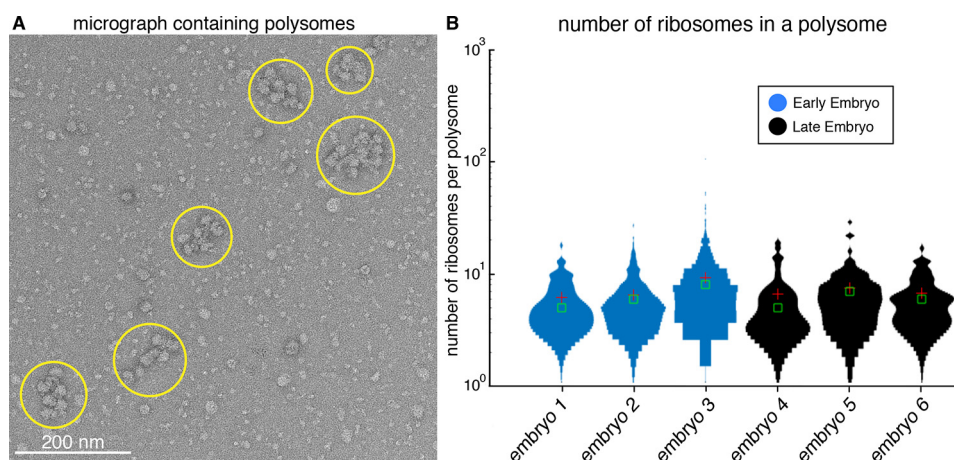
ASBMB

Figure 3. Counting ribosomes in polysomes from early- and late-stage *C. elegans* embryos. *A*, representative raw electron micrograph of negatively stained single-cell lysate showing several distinct polysome clusters of varying size (*yellow circles*). *B*, distribution of the number of ribosomes in a polysome across three early- and three late-stage embryos. The average numbers of ribosomes for early- and late-stage embryos are eight and seven, respectively. The *red cross-hair* is the mean value, and the *green box* is the median (n = 81, 513, 319, 31, 71, and 52 for embryos 1–6, respectively).

of ribosomes per polysome in our samples from each developmental stage. Each micrograph was manually annotated to determine the number of ribosomes per polysome cluster for our early-stage and late-stage embryos, respectively. Using this approach, we determined that there are, on average, eight ribosomes per polysome for early-stage embryos and seven ribosomes per polysome for late-stage embryos (Fig. 3*B*). These numbers are consistent with previous studies in which the number of ribosome per mRNA is estimated by isolating polysomes using velocity sedimentation in sucrose gradients (24), but our results add an additional dimension by observing polysomes at defined developmental stages that either have or lack zygotic transcription. Although our data suggested no significant change in the number of ribosomes per polysome between early and late stage embryos, this analysis provides evidence that single-particle counting from single cells could potentially be applied for investigating the dynamics of macromolecules in different cell states.

3D classification of ribosome particles from single embryo data

We then performed 3D classification of our large particles to determine whether any distinct structures could be obtained from lysates of single cells. Specifically, we were looking for structures of ribosomes because they appeared as clear and abundant 2D class averages in our data. We first combined two data sets from early-stage embryo samples for 3D classification using RELION (Fig. S3) (9). After removal of junk particles, ~14,000 particles were used for classification. Initially, we used an unbiased approach for 3D classification by using an initial model of a featureless 3D shape with uniform electron density. Using a model reconstructed from this initial classification, which resembled a previously determined 60S ribosome structure (25) (EMDB-2811) as a reference, we then performed another round of 3D classification (see "Experimental Procedures"). The models from each classification were then compared by docking a high-resolution *S. cerevisiae* 60S ribosome structure (EMDB-2811) into our maps to determine which class, if any, was most similar to the known structure. Our top
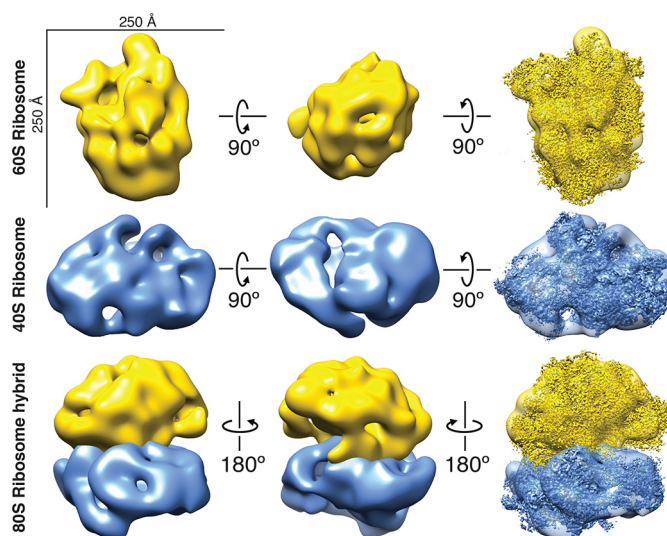

Figure 4. 40S and 60S ribosome reconstructions from particles from single cells. *Top row*, 60S ribosome reconstruction. High-resolution structure EMDB-2811 (25) docked into our 60S map with a cross-correlation score of 0.8142. *Middle row*, 40S ribosome reconstruction. High-resolution structure EMDB-4214 (26) docked in to our 40S map with a cross-correlation score of 0.8352. *Bottom row*, 80S ribosome hybrid model built using our 40S and 60S ribosome aligned to a high-resolution structure of the 80S ribosome EMDB-2858 (27).

scoring 60S ribosome reconstruction, containing ~3,400 particles, displayed striking similarity to the *S. cerevisiae* 60S ribosome (Fig. 4, *top row*) with a cross-correlation score of 0.8143 and a nominal resolution of 34 Å calculated using the 0.5 Fourier shell correlation criterion (Fig. S4) (see "Experimental Procedures").

Performing 3D classification on particles from all data sets combined, a final set of ~17,000 particles after stringent removal of junk particles resulted in an additional class that resembled the *S. cerevisiae* 40S ribosome (Fig. 4, *middle row*) (see "Experimental Procedures"). Our 40S ribosome reconstruction, containing ~1,450 particles, had a cross-correlation score of 0.8352 with the *S. cerevisiae* model (26) (EMDB-4214) and a nominal resolution of 48 Å (Fig. S4). These results suggest that 3D structures of multiple protein complexes can be

obtained from lysates of single embryos using single-particle EM analysis. To explore our ribosome reconstructions, we built a hybrid 80S ribosome model by aligning our 40S and 60S ribosome reconstructions to their respective domains in the 80S ribosome from a previously determined 80S ribosome structure (Fig. 4, *bottom row*) (27) (EMDB-2858). As expected, this hybrid model is consistent with the high-resolution 80S ribosome structure. Because of the limited number of proteasome particles in our sample, we did not attempt to obtain a 3D structure of the proteasome.

With clear structures resembling a 40S and 60S ribosome, we next attempted to determine the molecular architecture of the 80S ribosome directly from polysome clusters. Our data contained ~9,000 particles within polysomes that were manually picked for single-particle analysis. We then performed 2D and 3D classification of the selected particles (see "Experimental Procedures"). The 2D class averages were ~250 Å in diameter, which is consistent with the size of an *S. cerevisiae* 80S ribosome. Our 3D model, containing ~2,000 particles, had a cross-correlation score of 0.7572 when compared with an *S. cerevisiae* 80S ribosome (27) (EMDB-2858) and a resolution of 45 Å (Fig. S4). Although our 80S ribosome model lacked some areas of density present in the high-resolution structure, the overall size could accommodate both the 40S and 60S ribosome. Collectively, our data show that we are able to distinguish structures of the 40S, 60S, and 80S ribosomes directly from particles isolated from single cells.

Discussion

A major goal of basic biological research is to connect structural dynamics of macromolecules to their effects on cell behavior. Here, we present an approach for structural characterization of protein complexes isolated from single cells engaged in development. We demonstrate that a single cell contains a sufficient number of protein particles to enable structural characterization by EM. We think that this approach has significant potential to reveal structural changes in protein complexes across developmental and disease contexts. Our method is also promising for future single-cell cryo-EM, because the lysate transferring procedure can remain the same during cryo-EM sample preparation. The increased resolution from cryo-EM will help in the identification of other macromolecular complexes from lysate. However, we expect several obstacles moving our approach to cryo-EM including freezing small lysate volumes and capturing low-concentration proteins on grids.

Moving forward, a significant challenge will be to extend this approach beyond ribosomes and proteasomes to other macromolecular complexes. We focused here on ribosomes because they are large, highly abundant, and relatively easy to recognize. For complexes that are less abundant and/or less distinctive in shape, we will need to develop methods to identify a complex of interest in a heterogenous mixture. Correlative light and EM holds promise in this regard (28). We also plan to explore whether particles isolated and characterized via our earlier sc-SiMPull approach (5) can be eluted and transferred to EM grids for structural analysis. An added advantage of this strategy would be the ability to use multicolor TIRF to characterize the composition of complexes whose structures could then be

determined. Taken together, we are optimistic that these strategies will allow us to gain structural information about protein complexes beyond ribosomes and proteasomes using single-cell lysates.

A related question is whether there are enough particles in a single cell to allow high-resolution structure determination. This will of course depend on the protein or protein complex being studied; it may be more difficult to determine high-resolution structures of low-abundance complexes. However, we note that the time required to prepare and collect data from a single-cell sample is short enough that analyzing 10–20 such samples is realistic. Particles from multiple samples could be pooled to increase resolution, without sacrificing information about which cell each particle in the data set came from. This might represent an ideal compromise between the need for increased numbers of particles for structure determination and the desire for single-cell resolution for detailed developmental studies.

Experimental procedures

Microfluidic device fabrication

Microfluidic devices were fabricated using a standard soft lithography procedure. A photomask corresponding to the desired channel shape was designed using CAD software and produced by Cad-Art Services (Bandon, OR). An ~30-μm-thick layer of SU8–2025 photoresist was deposited on a plasma-treated silicon wafer by spin coating for 10 s at 400 rpm followed by 30 s at 2800 rpm and 30 s of deceleration. After soft baking at 65 °C for 3 min and 95 °C for 10 min, the films were exposed to 1000 mJ UV light through the photomask. Following a post-exposure bake of 5 min each at 95 °C and 120 °C, the molds were developed in SU8 developer (propylene glycol monomethyl ether acetate, PGMEA) and rinsed with isopropanol. The molds were hard baked at 95 °C for 30 min and then at 120 °C overnight.

PDMS (Sylgard 184 silicone elastomer kit, Dow Corning, Midland, MI) was mixed using a 10:1 ratio of base to curing agent and deposited onto the molds by spin coating at 400 rpm for 30s. The PDMS was cured for 20 min at 95 °C, then peeled off from the molds, and inlet and outlet holes were punched with a 2 mm biopsy punch. Each PDMS device contained 8 channels, and each channel was used for one single-embryo experiment.

24 × 60 mm glass coverslips were cleaned with ethanol and dried under nitrogen flow. Each cleaned coverslip was bonded to a PDMS device by 2 min of treatment with air plasma, then baked at 120 °C for 30 min to form a permanent bond.

The PDMS device was first activated by flowing 1 M KOH through the channels for 20 min, washed three times with water, and then dried. After activation, 2-[methoxy(polyethylenxy)9–12Propyl]-trimethoxysilane was applied to the channels for 30 min to prevent nonspecific protein binding. The channels were then washed three times with water and dried. The dry devices were cured overnight at room temperature and stored with the open holes facing downward, in a closed box, until use.

Sample preparation from staged embryos

WT *C. elegans* embryos (strain N2) were dissected from gravid adults in egg buffer (5 mM HEPES, pH 7.4, 118 mM NaCl, 40 mM KCl, 3.4 mM MgCl$_2$, 3.4 mM CaCl$_2$). Developmental stage was determined by visual inspection of morphology (cell shape and nuclear position) on a dissecting microscope. The embryo with desired stage was transferred to a 3-μl drop of lysis buffer (10 mM Tris, pH 8, 50 mM NaCl, 0.1% Triton X-100, 10% glycerol) and placed in the inlet well of a prepared microfluidic device using a mouth pipette. A clean 26-gauge needle was used to push the embryo into the microfluidic channel.

Once the embryo was trapped in the center of the chamber, the channel output was sealed with crystallography-grade clear tape (Crystal Clear, Hampton Research, Aliso Viejo, CA) to stop flow. The device was temporarily fixed under the dissecting microscope with the tape. The embryo was then immediately crushed while watching in the stereoscope, by pushing down on the surface of the PDMS with the melted tip of a glass Pasteur pipette. A clean glass needle connected to a 10-ml syringe through a short flexible tubing was used to puncture the top layer of the PDMS channel once the embryo lysed. The lysate (an approximate volume of 50 nl) was sucked into the needle and transferred onto a marked area of a glow discharged reference grid covered with carbon. Two to three different lysates were transferred onto different squares of the same grid, with no overlap. After the last embryo lysate was transferred, the grid was immediately negatively stained with five consecutive droplets of 2% (w/v) uranyl acetate solution, blotted to remove residual stain, and air-dried in a fume hood. Purified JNK2 (a gift from K. Dalby and N. Sun) was used in control experiments (33).

EM and data collection

Data were acquired using a JEOL 2010F transmission electron microscope operated at 200 keV with a nominal magnification of ×60,000 (3.6 Å at the specimen level). Each image was acquired using a 1-s exposure time with a total dose of $\sim$30–35 e$^-$ Å^{-2} and a defocus between −1 and −2 μm. A total of 1,402 micrographs from seven samples (three early embryos and four late embryos) were manually recorded on a Gatan OneView camera.

Seven independent particle stacks were generated from the micrographs of each sample: 341 micrographs of an early-staged embryo sample (E1), 350 micrographs of an early-staged embryo sample (E2), 250 micrographs of an early-staged embryo (E3), 100 micrographs of a late-staged embryo (L1), 111 micrographs of a late-staged embryo (L2), 147 micrographs of a late-staged embryo (L3), and 103 micrographs of a late-staged embryo (L4). FindEM (29) was used for template-based particle picking with a template selected from reference-free 2D class averages generated from $\sim$10,000 large particles which were manually picked from the E1 data set. In total, $\sim$81,600 particles were selected from template picking of all data sets. All image pre-processing was done in Appion (30). After removing junk particles, 17,070 particles remained for further processing. Particle box size was set to 576 × 576 Å. Reference-free 2D class averages were generated with 100 classes using RELION (9).

The 2D class averages of large particles in the embryo lysate were compared with those of purified 40S ribosomes, 60S ribosomes, and 26S proteasomes from *S. cerevisiae* (a gift from A. Johnson, S. Musalgaonkar, A. Matouschek, and C. Davis) using EMAN. The micrographs of the yeast ribosomes and proteasomes were taken using the TEM procedures above.

For our 40S ribosome reconstruction, 3D classification was performed using RELION to create 10 classes. We used the structure of a purified DNA-dependent protein kinase catalytic subunit as an arbitrary initial model after being low-pass filtered to 60 Å. The top scoring model when compared with the *S. cerevisiae* 40S ribosome structure (EMDB 4214) contained 1,466 particles.

For our 60S ribosome reconstruction, a similar strategy was followed. Two independent particle stacks from E1 and E2 were used. The contrast transfer function of each micrograph was estimated using CTFFIND4 (31). Approximately 37,200 particles were selected by template picking. After removing junk particles, 13,916 particles were left. Particle box size was set to 432 × 432 Å. Reference-free 2D class averages were generated with 100 classes. 3D classification was performed to create eight classes. The structure of a featureless 3D shape with uniform electron density was chosen as an initial model after low-pass filtering to 60 Å. A subsequent round of 3D classification was performed on the same data using a reconstructed 3D class that was most similar to the 60S ribosome as the new initial model. From this classification, the best of three classes was determined by comparison to a *S. cerevisiae* 60S ribosome structure (EMDB 2811) and contained 3,431 particles.

For our 80S ribosome reconstruction, an initial stack of $\sim$9,000 particles in polysome-like structures were manually selected from all data sets combined. After removing junk particles, 5,638 particles remained for subsequent 2D and 3D classification. Particle box size was set to 576 × 576 Å. Reference-free 2D class averages were generated with 200 classes. 3D classification was performed to create two classes. The top scoring model when compared with a *S. cerevisiae* 80S ribosome structure (EMDB 2858) contained 1,971 particles.

We additionally performed an initial characterization of small particles found in our micrographs. Using a template-free difference of Gaussian particle picker (32), $\sim$165,00 particles were selected from data sets E1 and E2. Particle box size was set to 216 × 216 Å. After removing junk particles, 126,095 particles were classified using reference-free 2D classification to generate 150 classes.

Data plotting

To plot the distribution of ribosomes per polysome, we used Violin Plots for plotting multiple distributions (distributionPlot.m) MATLAB function that is publicly available online at the MathWorks file exchange.

Single-cell structural biology

References

1. Kumar, P., Tan, Y., and Cahan, P. (2017) Understanding development and stem cells using single cell-based analyses of gene expression. *Development* **144,** 17–32 CrossRef Medline
2. Huang, B., Wu, H., Bhaya, D., Grossman, A., Granier, S., Kobilka, B. K., and Zare, R. N. (2007) Counting low-copy number proteins in a single cell. *Science* **315,** 81–84 CrossRef Medline
3. Kovarik, M. L., and Allbritton, N. L. (2011) Measuring enzyme activity in single cells. *Trends Biotechnol.* **29,** 222–230 CrossRef Medline
4. Dickinson, A. J., Armistead, P. M., and Allbritton, N. L. (2013) Automated capillary electrophoresis system for fast single-cell analysis. *Anal. Chem.* **85,** 4797–4804 CrossRef Medline
5. Dickinson, D. J., Schwager, F., Pintard, L., Gotta, M., and Goldstein, B. (2017) A single-cell biochemistry approach reveals PAR complex dynamics during cell polarization. *Dev. Cell.* **42,** 416–434.e11 CrossRef Medline
6. Beck, M., and Baumeister, W. (2016) Cryo-electron tomography: can it reveal the molecular sociology of cells in atomic detail? *Trends Cell Biol.* **26,** 825–837 CrossRef Medline
7. Galaz-Montoya, J. G., and Ludtke, S. J. (2017) The advent of structural biology *in situ* by single particle cryo-electron tomography. *Biophys. Rep.* **3,** 17–35 CrossRef Medline
8. Kühlbrandt, W. (2014) The resolution revolution. *Science* **343,** 1443–1444 CrossRef Medline
9. Scheres, S. H. (2012) RELION: implementation of a Bayesian approach to cryo-EM structure determination. *J. Struct. Biol.* **180,** 519–530 CrossRef Medline
10. Punjani, A., Rubinstein, J. L., Fleet, D. J., and Brubaker, M. A. (2017) cryoSPARC: algorithms for rapid unsupervised cryo-EM structure determination. *Nat. Methods* **14,** 290–296 CrossRef Medline
11. Kastritis, P. L., O'Reilly, F. J., Bock, T., Li, Y., Rogon, M. Z., Buczak, K., Romanov, N., Betts, M. J., Bui, K. H., Hagen, W. J., Hennrich, M. L., Mackmull, M. T., Rappsilber, J., Russell, R. B., Bork, P., *et al.* (2017) Capturing protein communities by structural proteomics in a thermophilic eukaryote. *Mol. Syst. Biol.* **13,** 936 CrossRef Medline
12. Verbeke, E. J., Mallam, A. L., Drew, K., Marcotte, E. M., and Taylor, D. W. (2018) Classification of single particles from human cell extract reveals distinct structures. *Cell Rep.* **24,** 259–268.e3 CrossRef Medline
13. Kemmerling, S., Arnold, S. A., Bircher, B. A., Sauter, N., Escobedo, C., Dernick, G., Hierlemann, A., Stahlberg, H., and Braun, T. (2013) Single-cell lysis for visual analysis by electron microscopy. *J. Struct. Biol.* **183,** 467–473 CrossRef Medline
14. Arnold, S. A., Albiez, S., Bieri, A., Syntychaki, A., Adaixo, R., McLeod, R. A., Goldie, K. N., Stahlberg, H., and Braun, T. (2017) Blotting-free and lossless cryo-electron microscopy grid preparation from nanoliter-sized protein samples and single-cell extracts. *J. Struct. Biol.* **197,** 220–226 CrossRef Medline
15. Zhan, X., Kook, S., Kaoud, T. S., Dalby, K. N., Gurevich, E. V., and Gurevich, V. V. (2015) Arrestin-3–dependent activation of c-Jun N-terminal kinases (JNKs). *Curr. Protoc. Pharmacol.* **68,** 2.12.1–2.12.26 CrossRef Medline
16. Hillier, L. W., Reinke, V., Green, P., Hirst, M., Marra, M. A., and Waterston, R. H. (2009) Massively parallel sequencing of the polyadenylated transcriptome of C. elegans. *Genome Res.* **19,** 657–666 CrossRef Medline
17. Gerstein, M. B., Lu, Z. J., Van Nostrand, E. L., Cheng, C., Arshinoff, B. I., Liu, T., Yip, K. Y., Robilotto, R., Rechtsteiner, A., Ikegami, K., Alves, P., Chateigner, A., Perry, M., Morris, M., Auerbach, R. K., *et al.* (2010) Integrative analysis of the *Caenorhabditis elegans* genome by the modENCODE project. *Science* **330,** 1775–1787 CrossRef Medline
18. Malyutin, A. G., Musalgaonkar, S., Patchett, S., Frank, J., and Johnson, A. W. (2017) Nmd3 is a structural mimic of eIF5A, and activates the cpGTPase Lsg1 during 60S ribosome biogenesis. *EMBO J.* **36,** 854–868 CrossRef Medline
19. Sone, T., Saeki, Y., Toh-e, A., Yokosawa, H. (2004) Sem1p is a novel subunit of the 26 S proteasome from *Saccharomyces cerevisiae*. *J. Biol. Chem.* **279,** 28807–28816 CrossRef Medline
20. Brandt, F., Etchells, S. A., Ortiz, J. O., Elcock, A. H., Hartl, F. U., and Baumeister, W. (2009) The native 3D organization of bacterial polysomes. *Cell* **136,** 261–271 CrossRef Medline
21. Afonina, Z. A., Myasnikov, A. G., Khabibullina, N. F., Belorusova, A. Y., Menetret, J.-F., Vasiliev, V. D., Klaholz, B. P., Shirokov, V. A., and Spirin, A. S. (2013) Topology of mRNA chain in isolated eukaryotic double-row polyribosomes. *Biochem. Biokhimiia* **78,** 445–454 CrossRef Medline
22. Edgar, L. G., Wolf, N., and Wood, W. B. (1994) Early transcription in *Caenorhabditis elegans* embryos. *Development* **120,** 443–451 Medline
23. Seydoux, G., and Fire, A. (1994) Soma-germline asymmetry in the distributions of embryonic RNAs in *Caenorhabditis elegans*. *Development* **120,** 2823–2834 Medline
24. Slavov, N., Semrau, S., Airoldi, E., Budnik, B., and van Oudenaarden, A. (2015) Differential stoichiometry among core ribosomal proteins. *Cell Rep.* **13,** 865–873 CrossRef Medline
25. Shen, P. S., Park, J., Qin, Y., Li, X., Parsawar, K., Larson, M. H., Cox, J., Cheng, Y., Lambowitz, A. M., Weissman, J. S., Brandman, O., and Frost, A. (2015) Rqc2p and 60S ribosomal subunits mediate mRNA-independent elongation of nascent chains. *Science* **347,** 75–78 CrossRef Medline
26. Scaiola, A., Peña, C., Weisser, M., Böhringer, D., Leibundgut, M., Klingauf-Nerurkar, P., Gerhardy, S., Panse, V. G., and Ban, N. (2018) Structure of a eukaryotic cytoplasmic pre-40S ribosomal subunit. *EMBO J.* **37,** e98499 CrossRef Medline
27. Cianfrocco, M. A., and Leschziner, A. E. (2015) Low cost, high performance processing of single particle cryo-electron microscopy data in the cloud. *eLife* 10.7554/eLife.06664 CrossRef Medline
28. Schorb, M., and Briggs, J. A. (2014) Correlated cryo-fluorescence and cryo-electron microscopy with high spatial precision and improved sensitivity. *Ultramicroscopy* **143,** 24–32 CrossRef Medline
29. Roseman, A. (2004) FindEM: a fast, efficient program for automatic selection of particles from electron micrographs. *J. Struct. Biol.* **145,** 91–99 CrossRef Medline
30. Lander, G. C., Stagg, S. M., Voss, N. R., Cheng, A., Fellmann, D., Pulokas, J., Yoshioka, C., Irving, C., Mulder, A., Lau, P.-W., Lyumkis, D., Potter, C. S., and Carragher, B. (2009) Appion: an integrated, database-driven pipeline to facilitate EM image processing. *J. Struct. Biol.* **166,** 95–102 CrossRef Medline
31. Rohou, A., and Grigorieff, N. (2015) CTFFIND4: Fast and accurate defocus estimation from electron micrographs. *J. Struct. Biol.* **192,** 216–221 CrossRef Medline
32. Voss, N. R., Yoshioka, C. K., Radermacher, M., Potter, C. S., and Carragher, B. (2009) DoG Picker and TiltPicker: software tools to facilitate particle selection in single particle electron microscopy. *J. Struct. Biol.* **166,** 205–213 CrossRef Medline
33. Shaw, D., Wang, S. M., Villaseñor, A. G., Tsing, S., Walter, D., Browner, M. F., Barnett, J., and Kuglstatter, A. (2008) The crystal structure of JNK2 reveals conformational flexibility in the MAP kinase insert and indicates its involvement in the regulation of catalytic activity. *J. Mol. Biol.* **383,** 885–893 CrossRef Medline

ASBMB